JMEPEG (2016) 25:3638–3645
DOI: 10.1007/s11665-016-2191-4

1059-9495/$19.00

The Effect of Ti on Microstructural Characteristics and Reaction Mechanism in Bonding of Al-Ceramic Composite

Li Juan, Wang Kehong, and Zhang Deku

(Submitted February 18, 2016; in revised form May 27, 2016; published online June 24, 2016)

The effect of Ti on microstructural characteristics and reaction mechanism in bonding of Al-Ceramic composite was studied. Ti and Al-Ceramic composite were diffusion welded at 550, 600, 700, 800, and 900 °C in a vacuum furnace. The microstructures and compositions of the interface layers were analyzed, and the mechanical properties and fracture morphology of the joints were examined. The results indicated that there was a systematic switch from Ti/$Ti_7Al_5Si_{12}$/composite at 600 °C and Ti/$TiAl_3$/$Ti_7Al_5Si_{12}$/composite at 700 °C to Ti/$Ti_7Al_5Si_{12}$/$TiAl_3$/$Ti_7Al_5Si_{12}$/composite at 800 °C and Ti/$Ti_7Al_5Si_{12}$/$TiAl_3$/composite at 900 °C. The formation of $TiAl_3$ at 700 and 800 °C depended on Al segregation, which was an uphill diffusion driven by chemical potential. The maximum shear strength was 40.9 MPa, found in the joint welded at 700 °C. Most joints fractured between $Ti_7Al_5Si_{12}$ and Al-Ceramic composite. In any case, $Ti_7Al_5Si_{12}$ was favorable for Al-Ceramic composite welding, which attached to Al-Ceramic composite, reducing the differences in physiochemical properties between SiC and metal, improving the mechanical properties of the joints and increasing the surface wettability of Al-Ceramic composite.

Keywords Al-Ceramic composite, diffusion, interfacial reaction, mechanism, Ti alloy

1. Introduction

Al-Ceramic composites (70 vol.% SiC particles and 30 vol.% Al) are widely used in aerospace, weaponry, and electronics due to its high strength, rigidity, thermal stability, wear resistance, as well as low density, thermal expansion coefficient (Ref 1, 2). The connection of Al-Ceramic composite is inevitable in its applications. However, the surfaces of Al-Ceramic composites are mostly covered with SiC particles, which largely reduce the wettability. Until now, the welding of Al-Ceramic composite has been rarely reported due to its poor weldability. The weldability of the Al-Ceramic composite is similar to both the SiC ceramic and the low-volume-fraction SiC_p/Al (10 to 55 vol.%).

In the past, many welding methods were used to join the low-volume-fraction SiC/Al composite together or with other metals. So far, low-volume SiC_p/Al composite has been successfully joined by arc welding (Ref 3, 4), laser welding (Ref 5, 6), electron beam welding (Ref 7, 8), and friction stir welding (Ref 9, 10). As reported, 17 vol.% SiC_p/2009Al was joined by solid-state ultrasonic spot welding (Ref 11); 15 vol.% SiC_p/2009Al was joined via friction stir welding (Ref 12); and titanium was joined to 70 vol.% SiC/A356 during the fabrication via low-pressure infiltration (Ref 13). Al-Ceramic composite contains a very high volume fraction of SiC particles, which may cause arc instability, electron beam instability, and extreme liquid metal deficiency. Meanwhile, its high hardness complicates friction stir welding. Thus, brazing and diffusion welding are the most appropriate methods for Al-Ceramic composite welding. One urgent problem to be solved is to design an appropriate filler metal for Al-Ceramic composite welding.

In the twentieth century, researchers did many works on the low-volume-fraction SiC_p/Al welding, but there was rare study on Al-Ceramic composite welding. As reported, the welding of 15 vol.% SiC_p/Al composite with Al-Si filler metal by tungsten inert gas (TIG) welding greatly depressed the harmful interfacial reaction between SiC and Al and improved the maximum tensile force of the welded joints up to 240 MPa (Ref 14). The vacuum brazing of 55 vol.% SiC_p/A356 composite with Al-Cu-Si-Mg-Ni filler metal led to the formation of sound joints and improved the maximum shear strength of the bonded composites up to 102 MPa (Ref 15). The plasma arc in situ welding of 10 vol.% SiC_p/Al with Ti-containing filler metal effectively prevented the harmful phase Al_4C_3, improved the fluidity of the molten pool, and efficiently enhanced the maximum tensile strength of the welded joints up to 265 MPa (Ref 16, 17). In a system of Al-Si-Ti active filler metals for Al_2O_{3sf}/Al composites, Ti was added to improve the wettability of Al metal matrix composites through introducing the interfacial reactions at the filler metal/matrix and filler metal/reinforcement interfaces (Ref 18). Despite these great achievements, it is still unknown whether the achievements are applicable for brazing and diffusion welding of SiC-rich Al-Ceramic composite. If applicable, the mechanism is still to be studied.

As reported, when SiC ceramic was brazed with Al-Si (Ref 19) and ZnAlMg (Ref 20) filler metal using an ultrasonic-assisted method, the maximum shear strength of the joints was 89 and 148 MPa, respectively. When C_f/SiC and Nb were brazed at 1593 K using a Co-Ti-Nb filler metal, the addition of Ti and Nb as active elements improved the maximum shear strength up to 187 MPa (Ref 21). When TiAl and C/SiC were brazed with TiH_2-Vi-B filler metal, TiH_2 decomposed into Ti and H_2 and the highly active Ti was utilized in the reaction with

Li Juan, Wang Kehong and **Zhang Deku,** School of Material Science and Engineering, Nanjing University of Science and Technology, Nanjing, China. Contact e-mail: wkh1602@126.com.

C/SiC composite (Ref 22). Also, Ag-Cu-Ti (Ref 23), Ti-Zr-Cu-Ni (Ref 24), and Cu-Sn-Ti (Ref 25) filler metals were used to braze SiC ceramic or its composites. Most of these filler metals contain Ti, an active element that reacts with the base materials. Usually, the welding of SiC ceramic with Ti-containing filler metals would lead to the formation of Ti_5Si_3, Ti_3SiC_2, $TiSi_2$, and TiC. These reactions largely affect the wettability and mechanical properties of the joints, and these brazing processes were usually executed within 800 to 900 °C.

As for the welding of SiC or SiC-containing materials, Ti was usually added as an active element into the filler metal (Ref 26, 27). But whether Ti addition is applicable for Al-Ceramic composite is still unknown. If yes, the effects of temperature and the mechanisms should be explored.

Before this work, we designed 25 types of Al-Si-Mg-Cu solders and their average wetting angles on the surface of Al-Ceramic composite is about 91.6°. We also designed another 9 types of Al-Si-Mg-Cu-Ti filler metals, and their average wetting angle is about 32.2°. The wetting angle of the ordinary Al-Si-Mg is 100° measured by the same method. Thus, Ti addition can obviously improve the wettability of the welding materials on the surface of Al-Ceramic composite.

In this work, the diffusion–reaction between Ti and Al-Ceramic composite were executed at different temperatures (550, 600, 700, 800, and 900 °C). The microstructures and compositions of the interface layers were analyzed. The properties and fracture morphology of the joints were examined. Mechanisms of the interfacial reactions between Ti an Al-Ceramic composite were discussed. The mechanism how Ti addition improves the wettability of Al-Ceramic composite was discussed by analyzing the diffusion–reaction mechanism.

2. Experimental Procedures

The base materials used in the experiments were Al-Ceramic composites (Al-70 vol.% SiC_p composite) and Ti-4Al-1.5Mn alloy (Al: 3.5 to 5.0 wt.%, Mn: 0.8 to 2.0 wt.%, Fe: ≤ 0.03 wt.% and Ti: Bal.). Al-Ceramic composite is produced by a vacuum pressure infiltration route. Before the preparation of Al-Ceramic composite, SiC particles in appropriate size were selected and covered with a Si layer in advance. After that, the pretreated SiC particles were mixed with a connecting agent and a pore-forming agent. Then the mixed powder was pressed into a block and sintered to form embryos. The porosity of the embryos was tested later, and only embryos with about 30% porosity were subjected to the vacuum pressure infiltration. At the pressure range of 1.5 to 2.0 MPa, the Al-Ceramic composites containing 70 vol.% SiC particles were obtained. During the application, Al-Ceramic composite was not broken unless the sintered SiC skeleton was broken. Thus, its heat pressing resistance is much stronger than Al alloy. The composites were machined to welding samples of 15 mm length, 5 mm width, and 5 mm thickness, while the Ti alloy plates were cut into welding samples of 15 mm length, 10 mm width, and 2 mm thickness by spark cutting. All of the to-be-joined surfaces were carefully ground with water emery paper and emery paper (grit 280, 320, 400, and 600) and ultrasonically cleaned in acetone at room temperature before welding. Then, the composite samples were put onto the Ti samples, and the assembled specimens were put into a vacuum heating pressing furnace. The experiment parameters included a constant strength of 10 MPa, a holding time of 1.5 h, a vacuum of 3.0 to 5.0×10^{-3} Pa, and temperatures of 550, 600, 700, 800, and 900 °C. The diffusion-welded joints were cut, perpendicular to the weld line, into two parts via electric spark cutting. One part was used for microstructure analysis and the other for mechanical property test. The specimens for microstructure analysis were prepared by emery paper grinding, diamond paste polishing, and etching. Scanning electron microscopy (SEM), energy dispersive spectrometer (EDS), and x-ray diffraction (XRD) were used for typical microstructure and composition analyses. The shear strength of the samples was measured using a special jig made of T10 steel (Fig. 1). The shear test was conducted with a constant speed of 0.1 mm/min at room temperature, using a universal testing machine. For reliable results, five samples, made under identical conditions, were tested each case.

3. Results and Discussion

3.1 Microstructure of the Joints

Figure 2 shows the microstructures and compositions of the Ti and Al-Ceramic composite joints diffusion welded at 550, 600, 700, 800, and 900 °C. Reliable joints were obtained at all the investigated temperatures. All the (a)s in Fig. 2 show the microstructures of the joints, the (d)s are other areas around the interface, the (b)s show the XRD results of the interfaces, and tables in (c)s show the compositions of the possible phases in (a)s and (d)s. As shown in Fig. 2, the width of the reaction layer increases greatly with the temperature rising to 700 °C and waved slightly above 700 °C, and the interface layers achieved at different temperatures were not the same.

Figure 2A shows the SEM, XRD, and EDS results for the joint welded at 550 °C. No reaction layer is observed in Fig. 2A-(a), indicating that there was rarely reaction happened. Figure 2A-(b) shows that Ti is the only phase detected, and the EDS analyses results are listed in Fig. 2A-(c). A few Si and Al atoms dissolved in the Ti alloy to form a Ti[Si,Al] solid solution. When Ti and Al-Ceramic composite were welded below 550 °C, no chemical reaction occurred and the combination between Ti and Al-Ceramic composite mainly depends on the diffusion of the atoms.

When elevating the welding temperature to 600 °C, a filmy reaction layer formed (Fig. 2B-(a)). XRD and EDS results show that the reaction layer is $Ti_7Al_5Si_{12}$ phase. The atomic percentages of Ti, Al, and Si were 54.75, 11.76, and 33.49 at.%, respectively, which slightly deviated from Ti 50 at.%, Al 20.83 at.%, and Si 29.17 at.%. During the diffusing welding process,

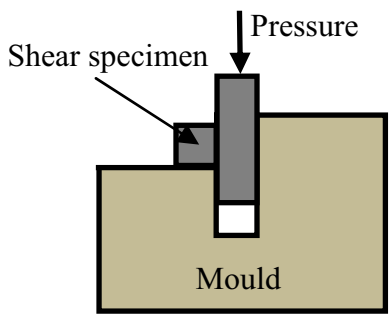

Fig. 1 Schematic diagram of the shear test

when the composition reached Al-11.7Si, the eutectic reaction happened. Due to gravity, a thin layer of Al-Si eutectic liquid gathered at the interface. Then Ti and Si diffused into the liquid to form $Ti_7Al_5Si_{12}$. Since Ti and Si were far more than Al in the system and their atomic radii were similar, a small amount of Ti and Si atoms dissolved into $Ti_7Al_5Si_{12}$ to take the place of Al, which led to the composition deviation of $Ti_7Al_5Si_{12}$. Si in $Ti_7Al_5Si_{12}$ came from SiC particles which were covered by Si before the Al-Ceramic composite was prepared.

With the temperature increasing to 700 °C, the reaction layer thickened gradually (Fig. 2C-(a)). The interface layers mainly included A_3 and B_3 phases. A_3 phase existed in partial regions as shown in Fig. 2C-(d). The composition of phase A_3 adjacent to the Ti side is similar to $TiAl_3$, which was proved by the XRD analysis, and Si atoms could dissolve into Al and take the place of Al atoms. It is reasonable to consider phase A_3 as $TiAl_3$. Phase B_3 was identified as $Ti_7Al_5Si_{12}$ with a small amount of Ti and Si atoms dissolved in.

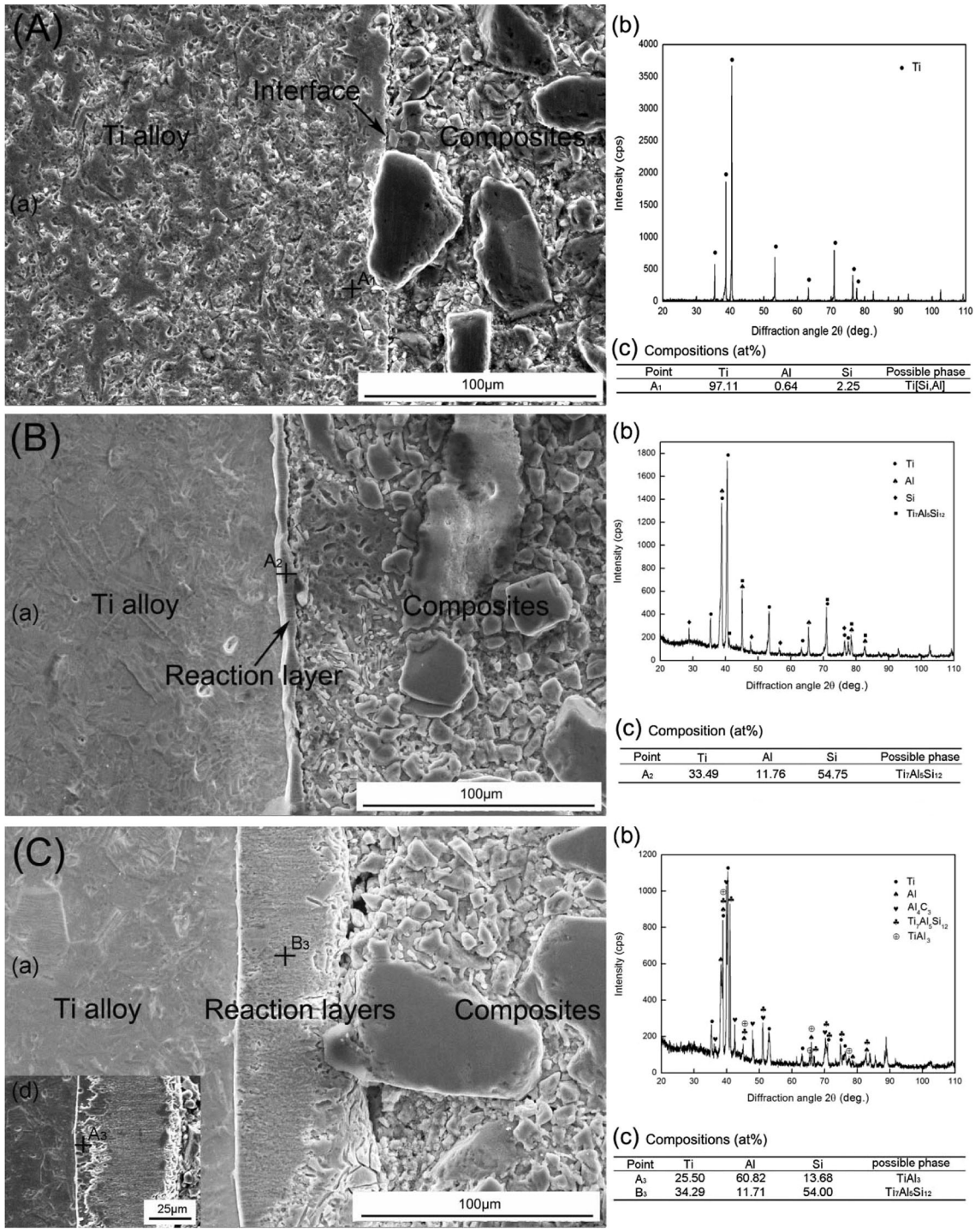

Fig. 2 SEM, EDS, and XRD results of the joints obtained at different temperatures: (A) 550 °C; (B) 600 °C; (C) 700 °C; (D) 800 °C; (E) 900 °C

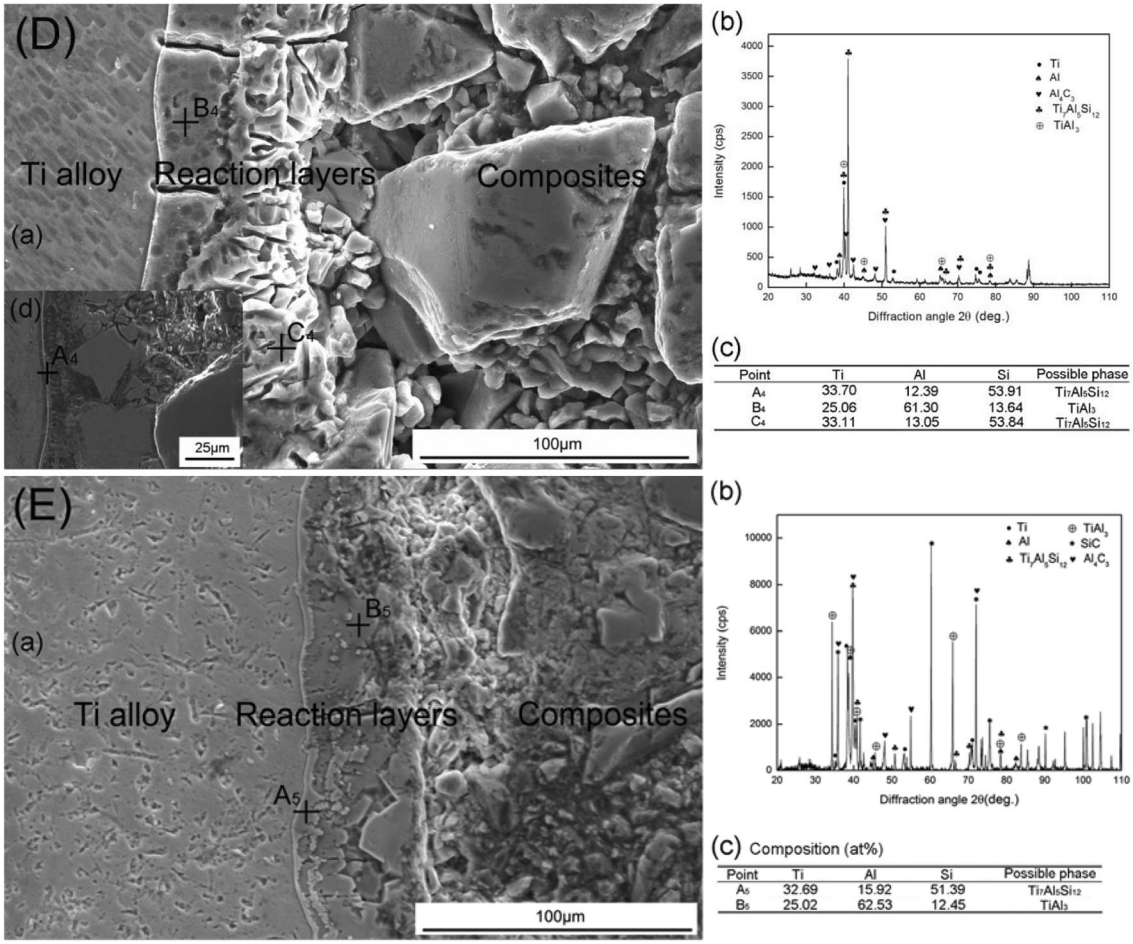

Fig. 2 contonued

Table 1 Phase compositions of the joints welded at different temperatures

Temperature, °C	Phase compositions of the reaction layers
550	No interface reaction
600	$Ti_7Al_5Si_{12}$
700	$TiAl_3$, $Ti_7Al_5Si_{12}$
800	$Ti_7Al_5Si_{12}$, $TiAl_3$, $Ti_7Al_5Si_{12}$
900	$Ti_7Al_5Si_{12}$, $TiAl_3$

When Ti and Al-Ceramic composite were welded at 800 °C, the interface layers are shown in Fig. 2D. According to the XRD and EDS results in Fig. 2D-(b) and (c), phase A_4 was $Ti_7Al_5Si_{12}$, B_4 was $TiAl_3$, and C_4 was $Ti_7Al_5Si_{12}$. When Ti and Al-Ceramic composite were welded at 900 °C, the reaction layers are shown in Fig. 2E. Phase A_5 was $Ti_7Al_5Si_{12}$, and B_5 was $TiAl_3$.

3.2 Mechanism of the Interfacial Reaction

Table 1 summarized the phase structures of the interface layers achieved at different temperatures. As Ti, Al, and Si were all solid at 550 °C, no interfacial reaction happened at that temperature, and the interfacial reaction at 600 °C was described above. What needs to be explained here is that there was a systematic switch from the order Ti/$TiAl_3$/$Ti_7Al_5Si_{12}$/composite at 700 °C to Ti/$Ti_7Al_5Si_{12}$/$TiAl_3$/$Ti_7Al_5Si_{12}$/composite at 800 °C and Ti/$Ti_7Al_5Si_{12}$/$TiAl_3$/composite at 900 °C.

Firstly, when Ti and Al-Ceramic composite were welded at 700 °C, Al-Si eutectic liquid occurred with the temperature rising, and a thick liquid film gathered at the interface due to gravity slowly. During the heat preservation process, Ti and Si atoms diffused from the base materials to the Al-Si liquid film. $Ti_7Al_5Si_{12}$ prior nucleated in the midregions of the film, where the composition was similar to that of $Ti_7Al_5Si_{12}$, and then it expanded to both sides. $Ti_7Al_5Si_{12}$ was generated in the heat preservation process. At the same time, Al segregated to the interface adjacent to the Ti side to form $TiAl_3$. The driving force of the segregation will be discussed later.

Secondly, when Ti and Al-Ceramic composite were welded at 800 °C, a small amount of $Ti_7Al_5Si_{12}$ (Phase A_4 in Fig. 2D-(d)) was generated during the heating process. The difference is that this $Ti_7Al_5Si_{12}$ was formed during the heating process, not the heat preservation process. During the heat preservation process, more Al liquid accumulated to the interface. At that time, Al segregated to the interface adjacent to Ti to form $TiAl_3$. Compared to the occasion at 700 °C, Al liquid film accumulated faster, and Ti and Al easily reacted to form $TiAl_3$ at 800 °C. That is why the $TiAl_3$ layer was thicker than the one achieved at 700 °C. At the same time, Ti atoms diffused into the liquid film adjacent to the Al-Ceramic composite to form more $Ti_7Al_5Si_{12}$ compound.

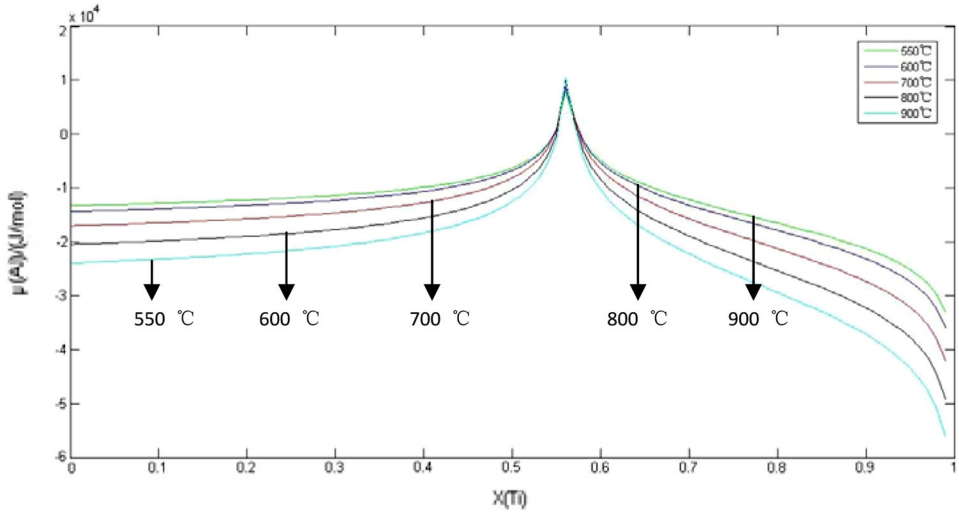

Fig. 3 The changing trend of μAl with the increase of Ti fraction

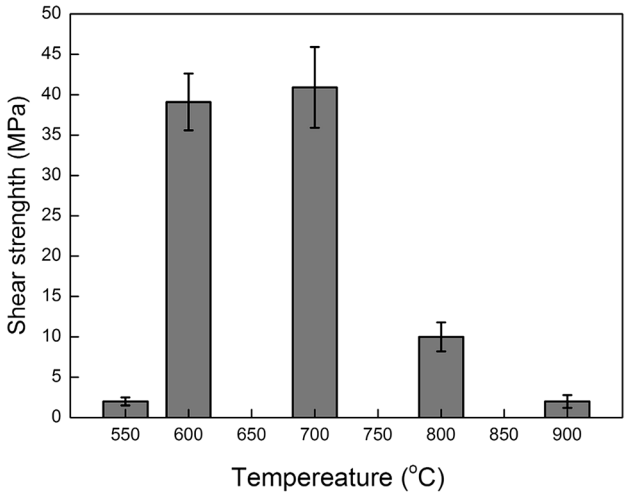

Fig. 4 Shear strength of the joints welded at different temperatures

Lastly, when Ti and Al-Ceramic composite were welded at 900 °C, a layer of continuous $Ti_7Al_5Si_{12}$ (Phase A_5 in Fig. 2E-(a)) was generated adjacent to the Ti alloy during the heating process, so the Ti atoms diffusing into the thick Al liquid film must go through this layer first, which largely decelerates the diffusion. Thus, Ti atoms in the Al liquid could not afford the formation of $Ti_7Al_5Si_{12}$. That is why there was rarely $Ti_7Al_5Si_{12}$ formed between the $TiAl_3$ layer and the Al-Ceramic composite.

In a word, 600 to 800 °C is an appropriate temperature range for active Ti to react with Si on SiC particle surfaces and Al to form $Ti_7Al_5Si_{12}$, which may enhance the connection between metals and Al-Ceramic composite.

As it is said in the introduction, if Ti can react with the surface of SiC particles at a certain temperature, it can improve the wettability on the surface of Al-Ceramic composite at this temperature. According to the analyses above, it can be inferred that Ti cannot improve the wettability on the surface of Al-Ceramic composite at 550 °C, but it can improve the wettability at 600, 700, 800, and 900 °C.

3.3 Chemical Potential Model

When Ti and Al-Ceramic composite were welded at 700 and 800 °C, the generation of $TiAl_3$ compound depended on the segregation of Al. During the segregation process, Al atoms were transferred from the enrichment area to the poor area, which was an uphill diffusion. The driving force for the uphill diffusion must be discussed.

An element's diffusion behavior depends on its chemical potential. Atoms were always transferred to the low chemical potential areas from the high ones. In this work, chemical potential of the Ti-Al-Si ternary alloy was calculated by the Miedema model and Toop model.

It was known that chemical potential is the partial molar free energy:

$$\mu_i = \frac{\partial G}{\partial x_i}, \quad \text{(Eq 1)}$$

where μ_i is the Chemical potential, x_i is the Mole fraction, and G is the System free energy.

The free energy consists of ideal free energy (G^I) and excess free energy (G^E).

$$G = G^I + G^E. \quad \text{(Eq 2)}$$

The free energy of ternary alloy is given in the following formula:

$$G^I = x_i G_i^* + x_j G_j^* + x_k G_k^* + RT[x_i \ln x_i + x_j \ln x_j + x_k \ln x_k] \quad \text{(Eq 3)}$$

where G_i^*, G_j^*, and G_k^* are the mole free energy.

According to the Toop equation,

$$G_{ijk}^E = \frac{x_j}{1-x_i} G_{ij}^E(x_i, 1-x_i) + \frac{1-x_i-x_j}{1-x_i} G_{ik}^E(x_i, 1-x_i) + (1-x_i)^2 G_{jk}^E\left(\frac{x_j}{1-x_i}, \frac{1-x_i-x_j}{1-x_i}\right), \quad \text{(Eq 4)}$$

where G_{ijk}^E is the free energy of i-j-k ternary alloy; G_{ij}^E, G_{ik}^E, and G_{jk}^E are the free energy of i-j binary alloy, i-k binary alloy, and j-k binary alloy, respectively.

$$G_{ij}^{E} = \Delta H_{ij} - T\Delta S_{ij}^{E}, \quad \text{(Eq 5)}$$

where ΔH_{ij} is the enthalpy of binary alloy, and ΔS_{ij}^{E} is the excess entropy of binary alloy.

According to Tanaka's theory,

$$\Delta S_{ij}^{E} = \Delta H_{ij}(1/T_{m,i} + 1/T_{m,j})/14, \quad \text{(Eq 6)}$$

where $T_{m,i}$, $T_{m,j}$ are the melt point.

Substituting Eq 6 into 5 gives

$$G_{ij}^{E} = \Delta H_{ij}\left[1 - \frac{T\left(\frac{1}{T_{m,i}} + \frac{1}{T_{m,j}}\right)}{14}\right]. \quad \text{(Eq 7)}$$

The derivations above indicate that the excess entropy of ternary alloy can be calculated from the excess entropy, and the excess entropy of binary alloy can be calculated from the enthalpy. According to the Miedema Model,

$$\Delta H_{ij} = f_{ij}\frac{x_i\left[1+\mu_i x_j\left(\varphi_i-\varphi_j\right)\right]x_j\left[1+\mu_j x_i\left(\varphi_j-\varphi_i\right)\right]}{x_i V_i^{2/3}\left[1+\mu_i x_j\left(\varphi_i-\varphi_j\right)\right]+x_j V_j^{2/3}\left[1+\mu_j x_i\left(\varphi_j-\varphi_i\right)\right]} \quad \text{(Eq 8)}$$

$$f_{ij} = 2pV_i^{2/3}V_j^{2/3} \times \frac{\frac{q}{p}\left(\Delta n_{ws}^{\frac{1}{3}}\right)^2 - (\Delta\varphi)^2 - a\frac{r}{p}}{\left(n_{ws}^{\frac{1}{3}}\right)_i^{-1} + \left(n_{ws}^{\frac{1}{3}}\right)_j^{-1}}, \quad \text{(Eq 9)}$$

where V_i, V_j are the molar volume, $(n_{ws})_i$, $(n_{ws})_j$ are the average electron density of Wigner–Seitz, φ_i, φ_j are the electronegativity, and p, q, r, μ, a are the empirical parameters.

The physical parameters and empirical parameters can be found in the literature (Ref 28). G^{I} can be calculated based on the free energy of Ti, Al, and Si according to Eq 3, G^{E} can be calculated according to Eq 4, and chemical potential can be calculated according to Eq 1 and 2.

It is a three-dimensional problem to discuss how the chemical potential was influenced by Ti, Al, and Si elements. According to the composition of Al-Ceramic composite, the proportion of Al and Si can be set as 30:70. With this limiting condition, the three-dimensional problem turns into an intuitive two-dimensional problem.

Figure 3 is the result of the chemical potential calculation that shows how the chemical potential of Al (μ_{Al}) changes with the Ti fraction (X_{Ti}) increasing. It can be seen that the chemical potential of Al increases with the increase of Ti fraction when

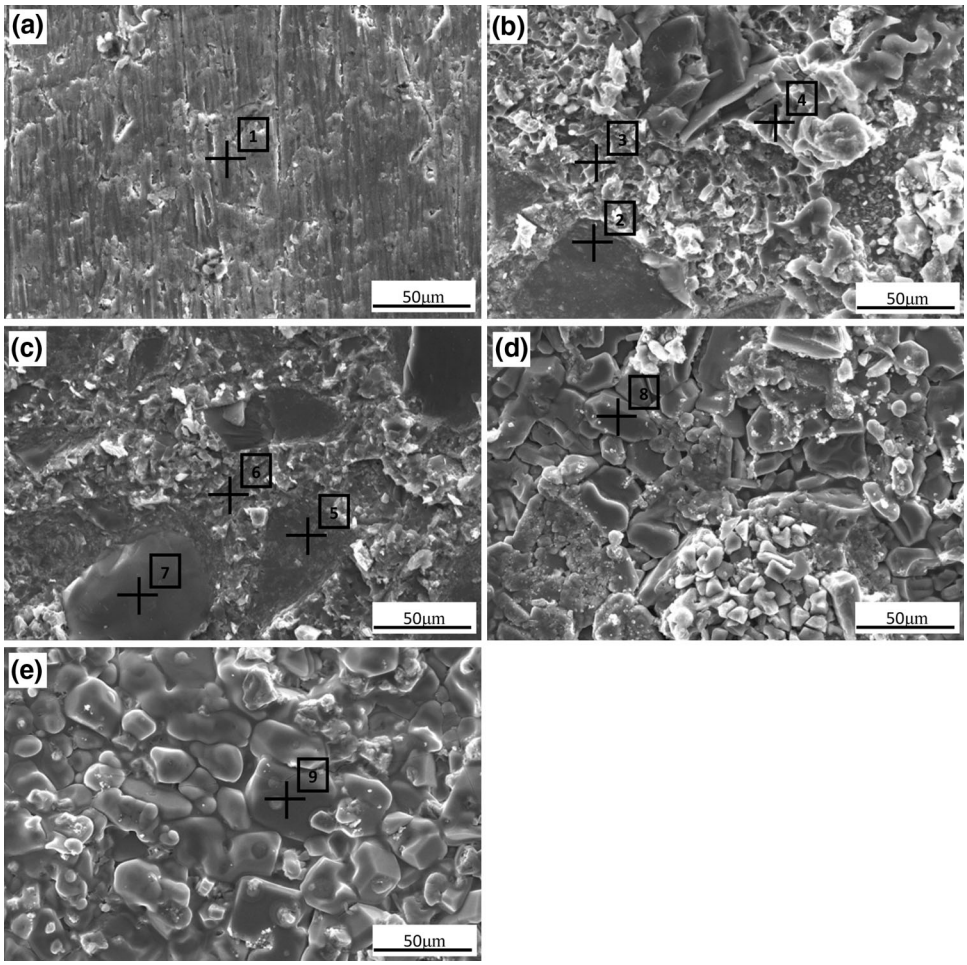

Fig. 5 Fracture morphology of the joints welded at different temperatures: (a) 550 °C, (b) 600 °C, (c) 700 °C, (d) 800 °C, (e) 900 °C

Table 2 EDS analyses of the points in Fig. 5 (at.%)

Element	Ti	Al	Si	C	Possible phase
Area 1	96.59	0.26	3.15		Ti[Si,Al]
Area 2	33.28	12.25	54.47		$Ti_7Al_5Si_{12}$
Area 3	27.14	31.05	41.81		$Ti_7Al_5Si_{12}$
Area 4	0.37	89.50	10.13		Al[Si,Ti]
Area 5	37.96	10.88	51.16		$Ti_7Al_5Si_{12}$
Area 6	26.56	17.97	55.47		$Ti_7Al_5Si_{12}$
Area 7		0.83	55.81	43.37	SiC
Area 8	34.77	13.23	52.00		$Ti_7Al_5Si_{12}$
Area 9	30.18	59.26	10.56		$TiAl_3$

Ti fraction is below 0.56 and decreases with the increase of Ti fraction when Ti fraction is above 0.56. At the initial stage of welding, x_{Ti} at the Ti-interface (the interface between Ti alloy and Al liquid film) was 1, and x_{Ti} at the composite interface (the interface between Al liquid film and Al-Ceramic composite) was 0. The value of μ_{Al} at the Ti-interface was greater than the one at the composite interface, so Al atoms were transferred from the composite to the Ti side. When $Ti_7Al_5Si_{12}$ was generated, the content of Ti was near 50%, and μ_{Al} in this area was very high, which drove Al atoms segregating to the Ti-interface. That can also explain the deficiency of Al in the $Ti_7Al_5Si_{12}$ compound.

3.4 Mechanical Properties and Fracture Characteristics of the Joints

Figure 4 shows the shear strength of the joints achieved at different temperatures. The results show that the joints welded at 700 °C had the maximum shear strength of 40.9 MPa. The shear strength of the joints was first increased with the temperature rising when it was welded below 700 °C, and then decreased with the temperature rising when it was welded above 700 °C.

Figure 5 shows the fracture morphology of the joints welded at different temperatures. The EDS results of the areas marked in Fig. 5 are listed in Table 2. At welding temperature 550 °C, the wear scars on the Ti alloy interface still exist (Fig. 5a). The EDS result shows the fracture was Ti alloy with some Al and Si atoms dissolved in. Metallurgical bonding between Ti alloy and Al-Ceramic composite did not appear. As the connection between Ti and Al-Ceramic composite mainly depended on the atom diffusion and the binding force was small, the shear strength of the joints welded at 550 °C was low.

The fracture morphology of the joint obtained at 600 °C is shown in Fig. 5(b). Areas 2, 3, and 4 in Fig. 5(b) were examined by EDS, and the results are shown in Table 2. Area 2 is $Ti_7Al_5Si_{12}$ adjacent to large SiC particles of the Al-Ceramic composite; Area 3 is $Ti_7Al_5Si_{12}$ adjacent to Al alloy and small SiC particles of the Al-Ceramic composite; Area 4 is Al alloy with a high volume of Si, torn off from Al-Ceramic composite. The fracture occurred at the interface between $Ti_7Al_5Si_{12}$ and Al-Ceramic composite with some Al alloys torn off from the composite.

Figure 5(c) shows the fracture characteristics of the joint welded at 700 °C. The EDS results of Areas 5, 6, and 7 are listed in Table 2. Areas 5 and 6 are $Ti_7Al_5Si_{12}$ and Area 7 is SiC which were examined by EDS. The SiC particles were peeled off from Al-Ceramic composite. The fracture of the joint occurs at the interface between $Ti_7Al_5Si_{12}$ and Al-Ceramic composite with some SiC particles peeled off from the composite, indicating that the binding force between $Ti_7Al_5Si_{12}$ and SiC at 700 °C is greater than the ones at other temperatures.

Figure 5(d) shows the fracture morphology of the joint achieved at 800 °C. The EDS of Area 8 shows that the fracture is mainly constituted by $Ti_7Al_5Si_{12}$. The $Ti_7Al_5Si_{12}$ compound, generated at 800 °C, has recrystallized which is obviously different from the morphology formed at 600 and 700 °C. The grain boundaries were not completely filled. The fracture belongs to brittle intergranular fracture.

Figure 5(e) shows the fracture characteristics of the joint welded at 900 °C. The EDS result of Area 9 shows that the joint fractured at the interface between $TiAl_3$ and Al-Ceramic composite which is completely different from the previous situations. The $TiAl_3$ grains on the fracture are all intact. The fracture also belongs to brittle intergranular fracture and the shear strength is extremely low.

Generally, $Ti_7Al_5Si_{12}$ is generated from the reaction between Ti, Al, and SiC (covered by Si) at the welding temperature above 600 °C, and could attach to the surface of Al-Ceramic composite. Thus, the generation of $Ti_7Al_5Si_{12}$ leads to a change from the "metal/SiC particles interface" to "metal/$Ti_7Al_5Si_{12}$/SiC particles interface," which can decrease the residual stress after welding, improve the wettability on the surface of Al-Ceramic composite, and enhance the welding quality.

4. Conclusions

(1) The interfacial reaction between Ti and Al-Ceramic composite happened at the welding temperature above 600 °C. There was a systematic switch from Ti/$Ti_7Al_5Si_{12}$/composite at 600 °C and Ti/$TiAl_3$/$Ti_7Al_5Si_{12}$/composite at 700 °C to Ti/$Ti_7Al_5Si_{12}$/$TiAl_3$/$Ti_7Al_5Si_{12}$/composite at 800 °C and Ti/$Ti_7Al_5Si_{12}$/$TiAl_3$/composite at 900 °C.

(2) The Miedema and Toop models were used to calculate the chemical potential of the Ti-Al-Si ternary alloy. The results indicated that the chemical potential of Al first increased with the increase of Ti fraction when Ti fraction was below 0.56, and then decreased with the increase of Ti fraction when Ti fraction was above 0.56. The segregation of Al at 700 or 800 °C was an uphill diffusing that was driven by chemical potential.

(3) The maximum shear strength of the joints is 40.9 MPa, found in the joint welded at 700 °C. The fracture of the joints occurred at the interface between $Ti_7Al_5Si_{12}$ and Al-Ceramic composite with some SiC particles peeled off from the composite.

(4) The generation of $Ti_7Al_5Si_{12}$ led to a systematic switch from the "metal/SiC particles interface" to "metal/$Ti_7Al_5Si_{12}$/SiC particles interface," which reduced the differences in physiochemical properties between SiC ceramic and metals, decreased the residual stress after welding, enhanced the welding quality, and improved the wettability on the surface of Al-Ceramic composite.

Acknowledgment

The work was supported by the weapons research fund project support (62201070813), the Natural Science Foundation of Jiangsu Province (BK20131261), the science and technology project of Jiangsu Province (BE2011194), and the graduate student training innovation project of Jiangsu Province (KYLX15_0413).

References

1. A. Zulfia and R.J. Hand, The Production of Al-Mg Alloy/SiC Metal Matrix Composites by Pressureless Infiltration, *J. Mater. Sci.*, 2002, **37**(5), p 955–961
2. J.M. Kunze and C.C. Bampton, Challenges to Developing and Producing MMCs for Space Applications, *JOM*, 2001, **53**(4), p 22–25
3. P.P. Lean, L. Gil, and A. Urena, Dissimilar Welds Between Unreinforced AA6082 and AA6092/SiC/25p Composite by Pulsed-MIG Arc Welding Using Unreinforced Filler Alloy, *Mater. Process. Technol.*, 2003, **143–144**, p 846–850
4. Y.C. Lei, W.J. Yuan, X.Z. Chen, F. Zhu, and X.N. Cheng, In-situ Weld-alloy Plasma Arc Welding of SiCp/Al MMC, *Trans. Nonferrous Met. Soc. China*, 2007, **17**, p 313–317
5. P. Bassani, C. Edoardo, C. Daniele, P. Barbara, and V. Maurizio, Effect of Process Parameters on Bead Properties of A359/SiC MMCs Welded by Laser, *Compos. Part A*, 2007, **38**, p 1089–1098
6. J.T. Niu, L.X. Pan, M.Z. Wang, C.B. Fu, and X.D. Meng, Research on Laser Welding of Aluminum Matrix Composite SiCw/6061, *Vacuum*, 2006, **80**, p 1396–1399
7. M.A. Chen, C.S. Wu, and Z.D. Zhou, Electron Beam Welding of SiC_p/LD2 Composite, *Trans. Nonferrous Met. Soc. China*, 2006, **16**, p 818–823
8. X.H. Ji, S.G. Wang, and G.P. Dong, Effects of Electron Beam Welding Parameters on SiC_p/101Al Welded Joints, *Rare Metal Mater. Eng.*, 2009, **38**(9), p 1650–1654
9. M. Bahrami, N. Helmi, K. Dehghani, and M.K.B. Givi, Exploring the Effects of SiC Reinforcement Incorporation on Mechanical Properties of Friction Stir Welded 7075 Aluminum Alloy: Fatigue Life, Impact Energy, Tensile Strength, *Mater. Sci. Eng. A*, 2014, **595**, p 173–178
10. M. Salehi, M. Saadamand, and J.A. Mohandesi, Optimization of Process Parameters for Producing AA6061/SiC Nanocomposites by Friction Stir Processing, *Trans. Nonferrous Met. Soc. China*, 2012, **22**, p 1055–1063
11. V.K. Patel, S.D. Bhole, D.L. Chen, D.R. Ni, B.L. Xiao, and Z.Y. Ma, Solid-state Ultrasonic Spot Welding of SiC_p/2009Al Composite Sheets, *Mater. Des.*, 2015, **65**, p 489–495
12. D. Wang, B.L. Xiao, Q.Z. Wang, and Z.Y. Ma, Friction Stir Welding of SiC_p/2009Al Composite Plate, *Mater. Des.*, 2013, **47**, p 243–247
13. C. Xue, J.K. Yu, and Z.Q. Zhang, In Situ Joining of Titanium to SiC/Al Composites by Low Pressure Infiltration, *Mater. Des.*, 2013, **47**, p 267–273
14. X.H. Wang, J.T. Niu, S.K. Guan, L.J. Wang, and D.F. Cheng, Investigation on TIG Welding of SiC_p-reinforced Aluminum-Matrix Composite Using Mixed Shielding Gas and Al-Si Filler, *Mater. Sci. Eng. A*, 2009, **499**, p 106–110
15. J.T. Niu, X.W. Luo, H. Tian, and J. Brnic, Vacuum Brazing of Aluminium Metal Matrix Composite (55 vol.% SiC_p/A356) Using Aluminium-based Filler Alloy, *Mater. Sci. Eng. B*, 2012, **177**(19), p 1707–1711
16. Y.C. Lei, H.L. Xue, W.X. Hu, and J.C. Yan, Effect of Ti-Si-Mg-Al Wire on Microstructure and Mechanical Properties of Plasma Arc In-situ Welded Joint of SiC_p/Al Composites, *Trans. Nonferrous Met. Soc. China*, 2012, **22**, p 305–311
17. Y.C. Lei, Z. Zhang, J.J. Nie, and X.Z. Chen, Effect of Ti-Al on Microstructures and Mechanical Properties of Plasma Arc In-situ Welded Joint of SiC_p/Al MMCs, *Trans. Nonferrous Met. Soc. China*, 2008, **18**, p 809–813
18. G.F. Zhang, W. Su, J.X. Zhang, and A. Suzumura, Development of Al-12Si-xTi System Active Ternary Filler Metals for Al Metal Matrix Composites, *Trans. Nonferrous Met. Soc. China*, 2012, **22**, p 596–603
19. X.G. Chen, R.S. Xie, Z.W. Lai, L. Liu, J.C. Yan, and G.S. Zou, Interfacial Structure and Formation Mechanism of Ultrasonic-assisted Brazed Joint of SiC Ceramics with Al-12Si Filler Metals in Air, *J. Mater. Sci. Tech.*, 2016, p 1–7
20. X.G. Chen, J.C. Yan, S.C. Ren, Q. Wang, J.H. Wei, and G.H. Fan, Microstructure, Mechanical Properties, and Bonding Mechanism of Ultrasonic-assisted Brazed Joints of SiC Ceramics with ZnAlMg Filler, *Ceram. Int.*, 2014, **40**, p 683–689
21. J. Zhang, Q. Zhang, C.F. Liu, G.C. Wang, and Y.H. Xuan, Effect of Brazing Temperature on Microstructure and Mechanical Properties of 2D C_f/SiC and Nb Joints Brazed with Co-Ti-Nb Filler Alloy, *Mater. Sci. Eng. A*, 2015, **634**, p 116–122
22. Z.W. Yang, L.X. Zhang, X.Y. Tian, Y.Z. Liu, P. He, and J.C. Feng, Interfacial Microstructure and Mechanical Properties of TiAl and C/SiC Joint Brazed with TiH2-Ni-B Brazing Powde, *Mater. Charact.*, 2013, **79**, p 52–59
23. Y. Liu, Z.R. Huang, and X.J. Liu, Joining of Sintered Silicon Carbide Using Ternary Ag-Cu-Ti Active Brazing Alloy, *Ceram. Int.*, 2009, **35**, p 3479–3484
24. B. Cui, J.H. Huang, C. Cai, S.H. Chen, and X.K. Zhao, Microstructures and Mechanical Properties of C_f/SiC Composite and TC4 Alloy Joints Brazed with (Ti-Zr-Cu-Ni) + W Composite Filler Materials, *Compos. Sci. Technol.*, 2014, **97**, p 19–26
25. S.X. Liu, B. Xiao, H.Z. Xiao, L.H. Meng, Z.Y. Zhang, and H.H. Wu, Characteristics of Al_2O_3/diamond/c-BN/SiC Grain Steel Brazing Joints Using Cu-Sn-Ti Active Filler Powder Alloys, *Surf. Coat. Technol.*, 2016, **286**, p 376–382
26. Y.X. Gu, Y.D. Zou, and W.D. Bai, *Ceramic and Metal Connection*, Press of Chemical Industry, Beijing, 2010, p 217
27. Y.H. Liu, *Preparation and Application of Metal Ceramic Materials*, Northeastern University Press, Shenyang, 2012, p 28–37
28. F.R. de Boer, R. Boom, W.C.M. Mattens, A.R. Miedema, and A.K. Niessen, *Cohesion in Metals—Transition Metal Alloys*, North-Holland, Amsterdam, 1989, p 699